Ultrasonics Sonochemistry 22 (2015) 272–277

Contents lists available at ScienceDirect

Ultrasonics Sonochemistry

journal homepage: www.elsevier.com/locate/ultson

Modeling the shear rate and pressure drop in a hydrodynamic cavitation reactor with experimental validation based on KI decomposition studies

Mandar P. Badve [a], Tibor Alpar [b], Aniruddha B. Pandit [a], Parag R. Gogate [a,*], Levente Csoka [b,*]

[a] Department of Chemical Engineering, Institute of Chemical Technology, Mumbai 400 019, India
[b] University of West Hungary, Institute of Wood Based Products and Technologies, 9400 Sopron, Hungary

ARTICLE INFO

Article history:
Received 2 May 2014
Received in revised form 22 May 2014
Accepted 22 May 2014
Available online 2 June 2014

Keywords:
Hydrodynamic cavitation
Simulation
Computational fluid dynamics
Weissler reaction
Shear rate

ABSTRACT

A mathematical model describing the shear rate and pressure variation in a complex flow field created in a hydrodynamic cavitation reactor (stator and rotor assembly) has been depicted in the present study. The design of the reactor is such that the rotor is provided with surface indentations and cavitational events are expected to occur on the surface of the rotor as well as within the indentations. The flow characteristics of the fluid have been investigated on the basis of high accuracy compact difference schemes and Navier–Stokes method. The evolution of streamlining structures during rotation, pressure field and shear rate of a Newtonian fluid flow have been numerically established. The simulation results suggest that the characteristics of shear rate and pressure area are quite different based on the magnitude of the rotation velocity of the rotor. It was observed that area of the high shear zone at the indentation leading edge shrinks with an increase in the rotational speed of the rotor, although the magnitude of the shear rate increases linearly. It is therefore concluded that higher rotational speeds of the rotor, tends to stabilize the flow, which in turn results into less cavitational activity compared to that observed around 2200–2500 RPM. Experiments were carried out with initial concentration of KI as 2000 ppm. Maximum of 50 ppm of iodine liberation was observed at 2200 RPM. Experimental as well as simulation results indicate that the maximum cavitational activity can be seen when rotation speed is around 2200–2500 RPM.

1. Introduction

Cavitation is the formation, growth and collapse of vaporous cavities in the liquid and typically high energy shock waves are generated due to the implosion of cavities. Pressures up to 1000 atm and temperatures up to 10,000 K can be reached locally over a microsecond interval due to the cavity collapse under conditions of water being used as medium [1]. Millions of such cavities form and collapse in the region where cavitation takes place which creates a number of small shock wave reactors locally under overall ambient conditions. The high energy release by implosion can be harnessed for useful effects such as chemical/physical transformations. There are mainly two types of cavitation viz. acoustic cavitation in which cavitation takes place in a liquid due to compression and rarefaction cycles of the propagating sound waves and hydrodynamic cavitation, in which flow geometry is altered in such a way that pressure in the fluid at certain point falls below its vapor pressure resulting in the formation of cavities. When cavitation takes place, highly reactive hydroxyl radicals are formed due to the dissociation of vapor trapped in cavitating bubbles, which are capable of chemical transformations [2]. Also shock waves generated due to cavitation are capable of breakage of chemical bonds and cell lysis. There have been various recent studies related to hydrodynamic cavitation being used for different applications such as wastewater treatment, cell disruption, chemical synthesis and biodiesel production [3–7].

In hydrodynamic cavitation, orifice or venturi are commonly used for the generation of cavitation, with possible variations in the geometric designs of orifice plates and venturi [8,9]. In addition, the high pressure and high speed homogenizers also generate cavitating conditions [10]. From the application point of view as well as for obtaining efficient design of cavitational reactors, it is very important to understand the physics behind the actual phenomenon of cavitation occurring inside the cavitational reactor. Various models have been proposed for the quantification of the chemical transformations and to establish a link between bubble behavior and chemical kinetics. Moholkar et al. [11] have

* Corresponding authors. Tel.: +91 22 33612024; fax: +91 22 33611020 (P.R. Gogate). Tel.: +36 99 518 305; fax: +36 99 518 302 (L. Csoka).
E-mail addresses: pr.gogate@ictmumbai.edu.in (P.R. Gogate), levente.csoka@skk.nyme.hu (L. Csoka).

http://dx.doi.org/10.1016/j.ultsonch.2014.05.017
1350-4177/

Nomenclature

C_v	cavitation number
D	outer diameter of the rotor (m)
F	volume force vector (N/m^3)
N	rotation speed of the rotor per second (RPS)
p	pressure (Pa)
P	power input (W)
Re	Reynolds number
u	velocity (m/s)
V	volume of the fluid (m^3)

Greek symbolsγ

	shear rate (s^{-1})
η	dynamic viscosity (Pa s)
v	kinematic viscosity (Pa s)
ρ	density of the liquid (kg/m^3)
τ	shear stress (Pa)

illustrated with the numerical simulations the role played by the turbulence in altering the single cavity behavior downstream of a cavitating orifice in a liquid flow. It has been established that bubble behavior changes drastically under turbulent conditions compared to non turbulent conditions and bubble behavior under turbulent condition is transient and resembles the behavior of a cavity under acoustic conditions. Gogate and Pandit [12] numerically studied the effect of various operating parameters such as the inlet pressure, initial cavity size, orifice diameter on dynamic cavity behavior. An empirical correlation was developed to anticipate the collapse pressure generated as a function of above mentioned parameters. Kanthale et al. [13] have used the cavity cluster (group of cavities) approach instead of a single cavity approach to understand the mechanism of cavitational effects. The effect of intensity, frequency of ultrasound and initial size of the cluster on pressure pulse generated by cavity cluster as well as the active cavitation zone has been investigated based on the bubble dynamics equations.

In the present study, a different type of hydrodynamic cavitating device comprising of a stator and rotor assembly has been modeled to predict the fluid flow pattern. A rotor rotates at very high speed in a confined annular space and liquid is passed through the gap between the stator and the rotor. Due to high speed of rotation, very high surface velocities are generated. Some indentations are also provided on the surface of the rotor. Liquid at high velocities enters the indentation due to the rotary action of the rotor and when liquid comes out of the indentation due to centrifugal flow, a low pressure region/vacuum is created near the upper surface of the indentations resulting into cavitation. At such high velocities of the liquid on the surface of the rotor, pressure drop across the surface of the rotor and indentation is sufficient enough for cavitation to occur and the magnitude of the pressure drop decides the cavitational intensity. In our previous work, the effectiveness of this type of setup for wastewater treatment [3] and for digestion (delignification) of wheat straw pulp [14] has been reported. Almost 90% reduction in COD of the wastewater was observed in the wastewater treatment study [3] and the mechanical properties of the paper hand sheets made from cavitationally treated pulp were found to be superior by almost 50–55% [14]. Although applicability of this type of setup for transformations has been tested, overall physics and the mechanism behind the generation of cavitation have not been fully realized. To address this issue and to analyze the phenomenon of cavitation inside such reactors, finite element simulation of the fluid flow inside the reactor has been investigated in the present study. The conception and scale-up of these reactors generally depend on the hydrodynamic characteristics (mainly water media) i.e., transport properties and enhanced mixing of the colloidal phases, heat and mass transfer characteristics and chemical kinetics of the reacting system. In this work, the application of finite element method to simulate fluid flow in a hydrodynamic cavitation reactor has been presented and the results of the simulation have been compared with the model reaction carried out to study the cavitational effects. The work presents useful design related information which would be very significant in getting optimum designs of large scale hydrodynamic cavitation reactors.

2. Experimental methodology and modeling details

2.1. Stator–rotor assembly

Fig. 1 shows schematic details of the stator–rotor assembly being used as the cavitating device. The rotor is attached to a gear assembly, which is connected to a variable frequency drive (VFD: YASKAWA J1000, type: CIMR-JC 4A0011BAA). With the help of VFD, the rotor can be rotated at different speeds of rotation. The rotor is a solid cylinder which has indentations/surface irregularities on its surface. There are a total of 204 indentations equidistant from each other. Each indentation is 12 mm in diameter and 20 mm deep. Gap between stator and rotor is fixed at 10 mm.

2.2. Experimental work

In order to analyze the behavior of cavitation inside this type of reactor, some experiments were carried out to quantify the cavitational effects. Weissler reaction, which has been used extensively as a model reaction for cavitation based transformations was also used in the present work [15]. Weissler reaction can be used to quantitatively analyze the degree of cavitational activity in the reactors. Weissler reaction is the decomposition of KI which liberates free iodine. Weissler reaction can be induced under cavitating and thermal oxidation conditions due to the fact that OH$^{\cdot}$ radicals are formed in the solution. In order to avoid the thermal oxidation of iodine, all the experiments were carried out at 25 °C and the volume of KI (2000 ppm initial concentration) solution taken was

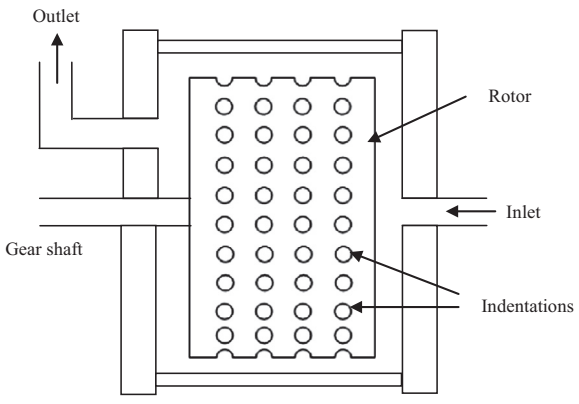

Fig. 1. Schematic of the cavitating device (stator and rotor assembly).

4 L for each experiment. Each experiment was carried out for 15 min and samples were drawn periodically to quantify the amount of iodine liberation. Experiments were carried out between the rotor speeds of 2000–3000 RPM. The extent of iodine liberated during the reaction is estimated with the help of a UV–VIS spectrophotometer by measuring the absorbance at 355 nm wavelength. The rate and the amount of the iodine liberation depend on the formation and supply of free OH· radicals, which are dependent on the degree of cavitational activity generated in the reactor.

2.3. Theoretical model considerations

Fluid motion in almost all types of reactors, mixers and reservoirs is governed by the conservation of mass, momentum and energy transport equations. The fluid considered in the present analysis is a Newtonian fluid under isothermal conditions. The model does not handle any inlet or outlet velocities and the pressure was set to 0 Pa at the periphery of the cylinder. In the model, no specific material was selected for the wall of the reactor and it was assumed that the mass fluxes due to the dispersion and diffusion are small; hence no mass of fluid can leave the fluid–solid interface.

In the model, the fluid is treated as a continuum and based on the Navier–Stokes momentum equation with no external forces, the following equation for the velocity and the pressure can be written:

$$\rho\frac{\partial u}{\partial t}+\rho(u\nabla)u=\nabla\left[-p\mathrm{I}+\eta(\nabla u+(\nabla u)^{T})\right]+F \tag{1}$$

where, u is the velocity (m/s), ρ is density (kg/m^3), η is dynamic viscosity (Pa s), p is the pressure (Pa) and F is the volume force vector (N/m^3).

The magnitude of Reynolds number was unknown at the start of the simulations. After the first calculation and evaluation of the model, the value of Reynolds number was such that the flow is laminar and shows non-compressibility. The obtained fluid density distribution was constant in the entire reactor. By fixing the velocity at each rotation, the viscosity changes can be calculated from the local pressure and shear rate as a post calculation method. Hence, the incompressibility constraint is handled by the div-stable velocity–pressure interpolations [16]. When the temperature changes in a flow are very small, a single phase flow can be assumed as non-compressible as well, having a constant density and the compressible continuity formulation can be expressed as:

$$\nabla u=0$$

Together with Stokes' assumption, the viscous stress tensor included in the above equation is based on the assumption that the fluid shows a Newtonian behavior. A normal flow is formally incompressible when the Mach number is zero or close to zero. The Navier–Stokes equation then has the numerical property that a disturbance anywhere in the computational domain instantaneously spreads to the entire domain. This results in a parabolic equation system, which is valid until the Mach number $\leqslant 1$. When the Mach number approaches 1, the parabolic equation needs to be replaced by hyperbolic set of equations to account for liquid phase compressibility and the boundary conditions of incompressible state become invalid. In our simulation, the maximum value for Mach number is 0.2 at 3000 rpm, which is the maximum speed of rotation considered in the modeling analysis and subsequent experimental validation. Mach number equal to 0.3 has been selected as the upper boundary in the simulation in order to avoid sharp gradients in the compressible Navier–Stokes equation and get rid of the sound wave transport term in the heat equation.

The specific energy absorption of the fluid in a rotating type reactor is dependent on the shear rate (γ) and shear stress (τ). Each fluid layer is subjected to the shear force due to the indentations on the rotating cylinder's surface. In Newtonian fluids, the shear rate (γ) and shear stress (τ) are related by the dynamic viscosity (μ) as follows:

$$\mu=\frac{\tau}{\gamma} \tag{2}$$

Considering the power input (P) and volume of the fluid (V), the shear rate is expressed as:

$$\gamma=\sqrt{\frac{P}{\mu V}}. \tag{3}$$

Because the viscosity and volume of the fluid are considered constant in the simulation, it can be concluded that the average shear rate of fluid showing Newtonian behavior is dependent on the rotational speed of the inner cylinder (rotor). Moreover, in the present case, viscous forces dominate and tend to damp all the disturbances, which finally lead to a laminar flow (because of the condition of the zero inlet and outlet velocities). The Reynolds number is defined as the ratio of inertial forces to the viscous forces which quantifies the relative importance of these types of forces. The Reynolds number can be calculated as per the equation given below [17]:

$$\mathrm{Re}=\frac{NH^2}{4v} \tag{4}$$

where, N is the rotation speed of the rotor, H is the gap width between rotor and stator and v is the kinematic viscosity. The Reynolds number varies from 0.142 (at 10 rpm) to 142.4 (at 10000 rpm) (Reynolds number at 3000 RPM is 42.6) which is still below the upper limit of laminar flow.

The mesh used in the present study is shown in Fig. 2. Both rotating sub domains are divided using tetrahedral elements. The computational domains involved are divided by rotational invariant geometries. Then the conservation equation is solved on rotating coordinate system to account for the indented cylinder. The outer cylinder is expressed in the fixed material coordinate system. An identity interface approach is involved to connect the rotating and standing zones together. This approach assumes that, at the interface, the flux continuity boundary condition is applied.

In general, Generalized Alpha algorithm is known to be accurate and faster for computation as compared to the Backward Differentiation Formulae (BDF) solver. Because of the complexity of the model, time step should be around 10^{-4} so that proper convergence is observed. The simulations were performed for a time span of 0.1 s.

In the current study, the rotating coordinate system allows the estimation of the shear rate and pressure drop as a function of rotational speed. The objective of the present study was to present the flow structure and quantify the shear rate and pressure drop for a given reactor configuration. The CFD results for single-phase fluid have been validated using the measured iodine liberation as a measure of the cavitational activity, since it is not possible to obtain velocity and pressure measurements using known techniques inside the cylinder.

3. Results and discussion

The velocity of liquid on the surface of the rotor will be altered by changing the speed of rotation of the rotor. Fig. 3 shows the effect of rotation speed on cavitation number. It can be seen from the Fig. 3 that surface velocities generated due to rotation of the rotor are sufficient for cavitation to occur. As the rotation speed

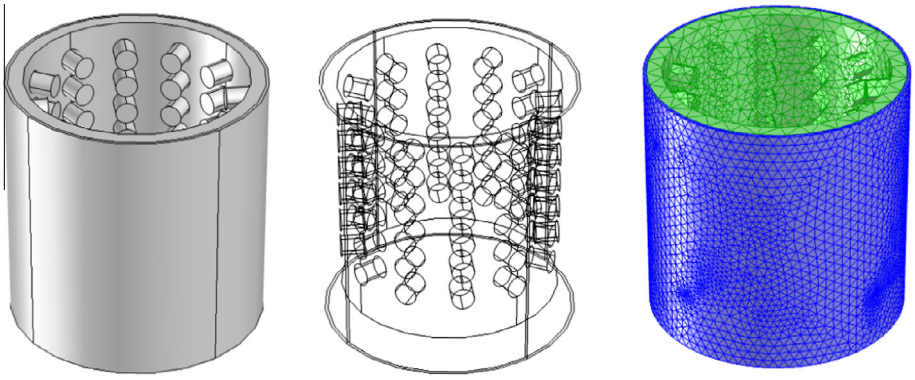

Fig. 2. Rotor–stator type hydrodynamic cavitator and mesh details in both subdomains.

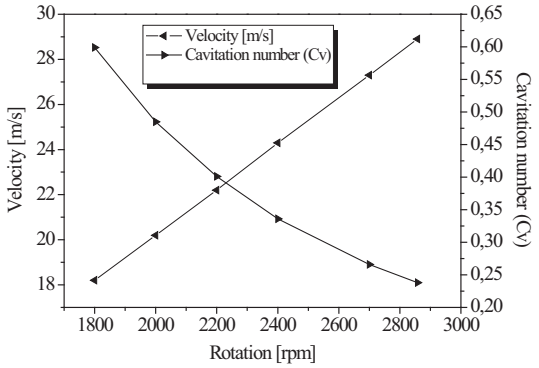

Fig. 3. Effect of rotation speed on surface velocities and cavitation number.

increases, the cavitation number decreases. It was observed in our previous work of wastewater treatment study [3] that the rate of reduction in COD changes with the change in cavitation number. It was observed also that a maximum 50% reduction in COD occurred at 2200 RPM at which C_V is around 0.4. Although the cavitation number decreases with further increase in the speed of rotation of the rotor, it was observed that the rate of reduction of COD decreases. This is because of the condition of choked cavitation. Similar observations are reported in the studies involving hydrodynamic cavitation [3,14].

3.1. Simulation and experimental results

Fig. 4 provides a detailed insight into the variation in streamlining patterns in the vicinity of an indentation as a function of speed of rotation. It can be seen that the difference among the rotations is conspicuous and more significant as the rotation speed is increased. Comparing the results for the lower (100 rpm) rotation situation with the higher (2000 rpm) rotation, taking into account the laminar flow, it can be said that the development of streamlines is more even, for 2000 rpm than 100 rpm attributed to the higher shear force. Up to the rotation speed of 100 rpm the vortices are defined by closed streamlines and it is observed that the emergence of vortices is dominant at lower (100 rpm) speed. The reason is that the forces are proportional to the rate of change of the fluid velocity vector as one moves away from the edge of the indentation or the reactor wall in various directions instantaneously inducing the generation of vortices. The number of emerging vortices increases with the number of indentations on the surface of the rotor. The generated velocity profile is parabolic in nature in the direction of rotation. It can also be seen that the indentation introduces an asymmetry in the vortex formed behind the indentation and also cause detachment in the homogenous streamline (as shown by arrows in the Fig. 4). This is because of the formation of an alleyway in front of the indentation. Due to the rotation and radial forces, the fluid is slightly drawn from the indentation as it is seen by the parabolic streamline profile (indicated by arrow). The width of that parabolic profile is shifted towards the wall and its magnitude increases as the rotation speed is increased. As the rotation speed increases, the intensity of the turbulence is also expected to increase and increase in the turbulence will be responsible for the generation of condition called transient cavitation. It has been generally agreed that cavitational based chemical transformation occurs only under a condition of transient cavitation and not under the condition of stable cavitation. Thus, the existence of turbulent conditions directly affects the cavitational yield. The yield may vary according to the extent of turbulence. Similar results are obtained in this study also. It can be seen that from Fig. 5 that as the rotation speed of the rotor increases from 2000 to 2200 RPM, the extent of iodine liberation increases from 40 to

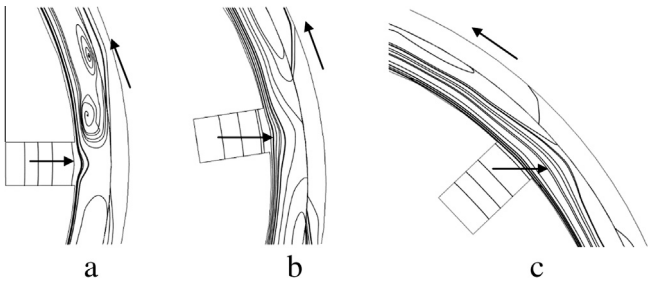

Fig. 4. (a–c) Steady streamlines near an indentation for various rotational velocities: (a) 100, (b) 2000, (c) 10000 rpm.

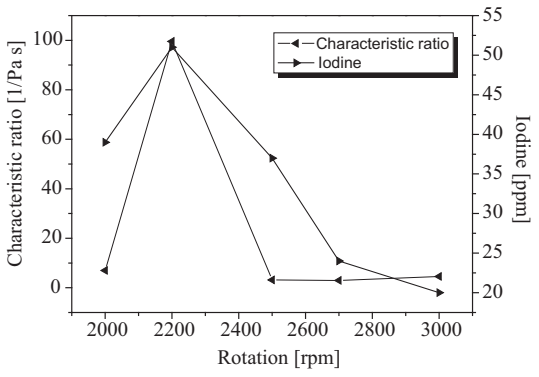

Fig. 5. Variation of characteristic ratio near an indentation and iodine liberation for various rotational velocities.

50 ppm. A further increase in the rotation speed, the extent of iodine liberation again decreases. This decrease in the liberation of iodine is due to the fact that as the rotation speed of the rotor increases beyond optimum the number density of cavities also increases and cavities tends to coalesce with each other forming cavity cloud [1]. Because of the formation of cavity cloud, energy release by a single cavity is damped by neighboring cavities which in turn reduces the intensity of cavitation and hence the reduction in rate of iodine liberation was observed. In order to illustrate why the lower pressure is the optimum operating condition, a characteristic ratio namely the shear rate divided by the pressure having a dimension of $Pa^{-1}\ s^{-1}$, which is reciprocal of viscosity, has been used in the analysis. This characteristic ratio is similar to Reynolds number and hence shows the relation between the viscous forces (shear rate) and the inertial forces (caused by pressure) in a reciprocal way. The shear rate increases with the rotation, but the pressure inside and around the indentation is a function of transient cavities, cloud formation or the natural frequency of travelling wave.

Fig. 6 shows the shear rate contours which illustrate the behavior of the forces as the rotation speed increases around an indentation. The maximum shear rate is observed at the trailing edge of the indentation. The effect of convection can be seen, though the movement and magnitude of the peak changes on the trailing edge of the indentation. This is consistent with the steady Poiseuille flow, which is a nothing but a shear flow. From the observations of both the peak shear rate as shown in Fig. 6 and the shear rate pattern at different rpm of the rotor, it can be established that the area of the high shear zone at the indentation's trailing edge is shrinking, but the magnitude of the shear rate increases with an increase in the rotation speed. Hence, it can be concluded that the rotation speed regulates the shear rate. At a higher rotation velocity, the indentation tends to stabilize the flow as the shear rate increases linearly.

The fluid in the indentation causes a repulsive force from the bottom in a radially outward direction forming a self-excited whirl. The whirl's motion is assumed to be parallel to the axis of fluid motion, exist only close to the indentation' edge and very short flow-transition exist in the surface wave of the fluid in the cylindrical reactor. The formation of the whirl in the laminar flow is developed in similar manner as the eccentrically channel-confined flow [18]. The modified shallow-water theory is applied here to interpret the relative pressure changes. Pressure changes inside and around an indentation has been depicted in Fig. 7. The maximum pressure is observed on the indentation's outward surface, while the lowest is observed at the bottom.

The equations of the first approximation of the shallow water theory are widely used to model the propagation of flow-transition waves on shallow water [19]. The method is based on a modified conservation law of total momentum that takes into account the

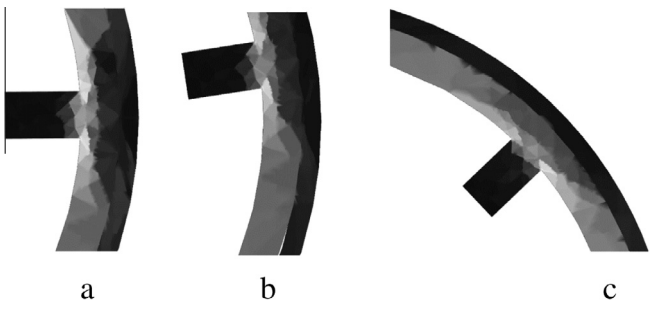

Fig. 6. Steady/instantaneous shear rate (1/s) contours near an indentation for various rotational velocities: (a) 100, (b) 2000, (c) 10000 rpm. (Note that black color represents low, white color high shear rates.)

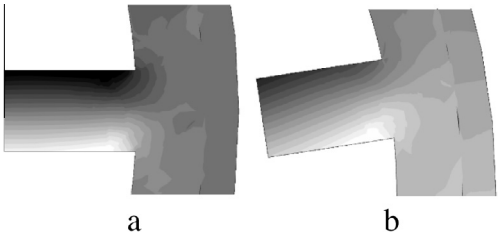

Fig. 7. Pressure distribution inside and around an indentation for the velocities at: (a) 100 and (b) 2000 rpm. (Note that black color represents low, white color high pressure field.)

concentrated momentum losses due to the formation of local turbulent vortex structures in the fluid surface layer at a transition-wave front. A quantitative estimate of these losses is obtained by deriving the shallow water equations from the Navier–Stokes equation with allowance for viscosity, which has a rapidly increasing effect on the flow distribution.

When the natural frequency of the indentation constrained surface wave (its frequency depends on the number of indentations and rotation speed) travelling on a fluid is close to the natural frequency of the elastically supported cylinder, it is a synchronous system. When this constrained surface wave travels slower than the rotation velocity the system becomes asynchronous. Above that point the delay between the rotation velocities is increasing rapidly. It is very difficult to calculate or predict the stationary amplitude or frequency of the asynchronous whirl, because there are transitions in the wave and the viscosity reduces that amplitude. The local hotspots, cavities and shear rate change the viscosity due to the temperature and pressure changes locally and hence those alter the amplitude of the travelling waves.

On the other hand, inertial forces between the standing and rotating cylinders tend to destabilize the fluid flow, whereas viscous forces tend to damp out the vortices. This ratio between the viscous and inertial forces is expressed by the dimensionless Taylor number and has a critical value around 1700. Taylor number characterizes the importance of centrifugal forces or so called inertial forces due to rotation of fluid about an axis, relative to viscous forces. When the Taylor number exceeds a critical value, inertial instabilities set in, which may lead to Taylor vortices or cells. Taylor number changes very rapidly with an increase in the angular velocity and reaches the critical value between 1800 and 2200 rotation as the pressure plot changes. As shown in Fig. 5, the relative pressure value at 2200 RPM suddenly decreases because of which overall pressure gradient increases. Due to these changes, the overall cavitation number will decrease which explains improved cavitational activity. It can also be seen from the experimental data that at 2200 RPM, maximum iodine liberation of (50 ppm) was observed compared to the iodine liberation at other rotational speeds.

4. Conclusions

The contribution of this work is to present a mathematical model describing the shear rate and pressure variation for the complex flow fields in a hydrodynamic cavitation reactor. The properties of fluid flow in hydrodynamic cavitation reactor are investigated on the basis of high accuracy compact difference schemes and Navier–Stokes method. The rotation evolutions of streamlining structure, pressure field and shear rate of a Newtonian fluid flow in the hydrodynamic cavitation reactor are numerically established. The results indicate that the characteristics of shear rate and pressure field are quite different at lower and higher speeds of rotation. It is shown that the pressure reaches a local

maximum level between 2000 and 3000 RPM and the isotropic streamline structure of fluid flow develops faster than the pressure changes. It has been established that the speed of rotation plays an important role on fluid flow, giving rise to the pressure changes and mass transfer of fluid flow in the reactor. It can be found additionally that the number of generating vortices is higher at lower rotations. Moreover, with a comparison of the related experimental data, it is demonstrated that the numerical results are valid. The present work has clearly illustrated the approach for optimizing the design of the hydrodynamic cavitation reactor based on the numerical modeling supported with experimental verifications.

Acknowledgement

This work was supported in part by the TET_13_DST-1-2014-0009 Inter-Governmental Science and Technology Cooperation Program and part of MTA Bolyai scholarship program. The financial supports are gratefully acknowledged.

References

[1] L.H. Thompson, L.K. Doraiswamy, Sonochemistry: science and engineering, Ind. Eng. Chem. Res. 38 (1999) 1215–1249.
[2] T.G. Leighton, The Acoustic Bubble, Academic Press, London, UK, 1994.
[3] M. Badve, P. Gogate, A. Pandit, L. Csoka, Hydrodynamic cavitation as a novel approach for wastewater treatment in wood finishing industry, Sep. Purif. Technol. 106 (2013) 15–21.
[4] M. Capocelli, D. Musmarra, M. Prisciandaro, A. Lancia, Chemical effect of hydrodynamic cavitation: simulation and experimental comparison, AIChE J. (in press), doi: 10.1002/aic.14472.
[5] M. Zupanc, T. Kosjek, M. Petkovšek, M. Dular, B. Kompare, B. Širok, M. Stražar, E. Heath, Shear-induced hydrodynamic cavitation as a tool for pharmaceutical micropollutants removal from urban wastewater, Ultrason. Sonochem. 21 (2014) 1213–1221.
[6] A.G. Chakinala, P.R. Gogate, A.E. Burgess, D.H. Bremner, Industrial wastewater treatment using hydrodynamic cavitation and heterogeneous advanced Fenton processing, Chem. Eng. J. 152 (2009) 498–502.
[7] K.P. Mishra, P.R. Gogate, Intensification of degradation of Rhodamine B using hydrodynamic cavitation in the presence of additives, Sep. Purif. Technol. 75 (2010) 385–391.
[8] Z. Dong, Q. Chen, Y. Yang, B. Shi, Experimental and numerical study of hydrodynamic cavitation of orifice plates with multiple triangular holes, Appl. Mech. Mater. 256–259 (2013) 2519–2522.
[9] E.F. Karamah, I. Sunarko, Disinfection of bacteria *Escherichia coli* using hydrodynamic cavitation, Int. J. Technol. 4 (2013) 209–216.
[10] K.K. Jyoti, A.B. Pandit, Water disinfection by acoustic and hydrodynamic cavitation, Biochem. Eng. J. 7 (2001) 201–212.
[11] V.S. Moholkar, A.B. Pandit, Bubble behavior in hydrodynamic cavitation: effect of turbulence, AIChE J. 43 (1997) 1641–1648.
[12] P.R. Gogate, A.B. Pandit, Engineering design methods for cavitation reactors II: hydrodynamic cavitation, AIChE J. 46 (2000) 1641–1649.
[13] P.M. Kanthale, P.R. Gogate, A.B. Pandit, A.M. Wilhelm, Cavity cluster approach for quantification of cavitational intensity in sonochemical reactors, Ultrason. Sonochem. 10 (2003) 181–189.
[14] M.P. Badve, P.R. Gogate, A.B. Pandit, L. Csoka, Hydrodynamic cavitation as a novel approach for delignification, Ultrason. Sonochem. 21 (2014) 162–168.
[15] A. Weissler, H.W. Cooper, S. Snyder, Chemical effect of ultrasonic waves: oxidation of potassium iodide solution by carbon tetrachloride, J. Am. Chem. Soc. 72 (1950) 1769–1775.
[16] R.C. Rovira, A finite element model for incompressible flow problems (Doctoral thesis), Barcelona, 1992.
[17] C.J. Butler, G.J. Sheard, K. Ryan, Modelling variations in shear rate around a geometrically similar thrombus in-vitro, Seventh International Conference on CFD in the Minerals and Process Industries CSIRO, Melbourne, Australia, 9–11 December 2009, 1–6.
[18] K. Prasad, A. Agrawal, A. Sharma, Poiseuille flow across an eccentrically confined stationary/rotating cylinder, Ocean Eng. 73 (2013) 41–54.
[19] V.V. Ostapenko, The propagation of discontinuous waves over a dry bed, J. Appl. Mech. Phys. 48 (2007) 795–812.